Loss of pim1 imposes a hyperadhesive phenotype on endothelial cells

Walpen, Thomas ; Peier, Martin ; Haas, Elvira ; Kalus, Ina ; Schwaller, Jürg ; Battegay, Edouard ; Humar, Rok

Abstract: Background: PIM1 is a constitutively active serine-threonine kinase regulating cell survival and proliferation. Increased PIM1 expression has been correlated with cancer metastasis by facilitating migration and anti-adhesion. Endothelial cells play a pivotal role in these processes by contributing a barrier to the blood stream. Here, we investigated whether PIM1 regulates mouse aortic endothelial cell (MAEC) monolayer integrity. Methods: Pim1-/-MAEC were isolated from Pim1 knockout mice and used in trypsinization-, wound closure assays, electrical cell-substrate sensing, immunostaining, cDNA transfection and as RNA source for microarray analysis. Results: Pim1-/-MAEC displayed decreased migration, slowed cell detachment and increased electrical resistance across the endothelial monolayer. Reintroduction of Pim1- cDNA into Pim1-/-MAEC significantly restored wildtype adhesive characteristics. Pim1-/–MAEC displayed enhanced focal adhesion and adherens junction structures containing vinculin and -catenin, respectively. Junctional molecules such as Cadherin 13 and matrix components such as Collagen 6a3 were highly upregulated in Pim1-/- cells. Intriguingly, extracellular matrix deposited by Pim1-/- cells alone was sufficient to induce the hyperadhesive phenotype in wildtype endothelial cells. Conclusion: Loss of Pim1 induces a strong adhesive phenotype by enhancing endothelial cell-cell and cell-matrix adhesion by the deposition of a specific extracellular matrix. Targeting PIM1 function therefore might be important to promote endothelial barrier integrity.

DOI: https://doi.org/10.1159/000341484

Cellular Physiology and Biochemistry

Cell Physiol Biochem 2012;30:1083-1096
DOI: 10.1159/000341484
Published online: September 24, 2012
Accepted: September 01, 2012

1015-8987/12/0304-1083$38.00/0

Original Paper

Loss of *Pim1* Imposes a Hyperadhesive Phenotype on Endothelial Cells

Thomas Walpen[a] Martin Peier[a] Elvira Haas[a] Ina Kalus[a] Jürg Schwaller[b] Edouard Battegay[a,c] Rok Humar[a,c]

[a]Research Unit, Division Internal Medicine, University Hospital Zürich, Zürich; [b]Department of Biomedicine, University of Basel, Basel; [c]Zurich Center for Integrative Human Physiology (ZIHP), Zürich

Key Words
Endothelial cells • Cell adhesion • PIM1 • Extracellular matrix • Cell migration

Abstract
Background: PIM1 is a constitutively active serine-threonine kinase regulating cell survival and proliferation. Increased PIM1 expression has been correlated with cancer metastasis by facilitating migration and anti-adhesion. Endothelial cells play a pivotal role in these processes by contributing a barrier to the blood stream. Here, we investigated whether PIM1 regulates mouse aortic endothelial cell (MAEC) monolayer integrity. ***Methods:*** *Pim1*$^{-/-}$MAEC were isolated from *Pim1* knockout mice and used in trypsinization-, wound closure assays, electrical cell-substrate sensing, immunostaining, cDNA transfection and as RNA source for microarray analysis. ***Results:*** *Pim1*$^{-/-}$MAEC displayed decreased migration, slowed cell detachment and increased electrical resistance across the endothelial monolayer. Reintroduction of *Pim1*-cDNA into *Pim1*$^{-/-}$MAEC significantly restored wildtype adhesive characteristics. *Pim1*$^{-/-}$-MAEC displayed enhanced focal adhesion and adherens junction structures containing vinculin and β-catenin, respectively. Junctional molecules such as *Cadherin 13* and matrix components such as *Collagen 6a3* were highly upregulated in *Pim1*$^{-/-}$ cells. Intriguingly, extracellular matrix deposited by *Pim1*$^{-/-}$ cells alone was sufficient to induce the hyperadhesive phenotype in wildtype endothelial cells. ***Conclusion:*** Loss of *Pim1* induces a strong adhesive phenotype by enhancing endothelial cell-cell and cell-matrix adhesion by the deposition of a specific extracellular matrix. Targeting PIM1 function therefore might be important to promote endothelial barrier integrity.

Rok Humar

Division Internal Medicine
Gloriastrasse 30/ GLO30-J14, 8091 Zürich (Schweiz)
Tel. +41 (0)44 634 53 85, Fax +41 (0)44 634 53 39, E-Mail Rok.Humar@usz.ch

Introduction

PIM1 is a constitutively active serine threonine kinase [1] and belongs to the family of kinases consisting of 3 members, PIM1 to 3 [2-4]. Mice deficient for all three *Pim* kinases displayed reduced body size and impaired responses to hematopoietic growth factors [5], suggesting that PIM kinases, including PIM1, are important but dispensable factors for growth factor signaling. At a molecular level, PIM1 promotes cell growth, migration, differentiation and survival through phosphorylation of several substrates, including $p21^{Cip1/WAF1}$ and BAD [6].

Elevated *Pim1* mRNA and protein levels correlated with the metastatic potential of tumors by facilitating migration and anti-adhesion as shown in tongue squamous cell carcinoma [7], gastric cancer [8] and in lymph node metastasis [9]. Vice versa, inhibition of PIM1 kinase activity diminished cancer cell migration and invasion *in vitro* [9, 10].

PIM1 is transiently expressed *in vivo* in endothelial cells during angiogenesis and induced by Vascular Endothelial Growth Factor (VEGF) in human umbilical vein endothelial cells (HUVECs). PIM1 silencing impaired vascular endothelial growth factor-A (VEGF-A) induced proliferation and migration and inhibited capillary formation on matrigel and endothelial cell sprouting in HUVECs [11].

Interactions between tumor cells and vascular endothelium are important for cancer metastasis [12]. Angiogenesis is not only a prerequisite for tumor growth but also promotes and facilitates migration, invasion and metastatic spread of malignant cells [13, 14]. In solid tumors, a prerequisite for cancer cell extravasation is alteration of endothelial cell barrier function, known to be associated with change in expression of molecules important for endothelial cell adhesion [15-17]. Here, we have investigated the specific contribution of PIM1 in endothelial cell adhesion at a functional, molecular and gene regulatory level.

Materials and Methods

Cell culture & transfection

MAECs were isolated from aortae of FVB/N wildtype and *Pim1*$^{-/-}$ mouse strains as described previously [18]. For all experiments cell culture dishes were precoated with 0.1% gelatine gold (Carl Roth GmbH, Karlsruhe, Germany) for 20 minutes at 37°C. Cells were maintained in DMEM (Biochrom, Berlin, Germany) complemented with 10% FBS, 1% sodium pyruvate, 1% non-essential amino acids and 1% penicillin-streptomycin (Invitrogen, LuBioScience GmbH, Luzern, Switzerland). Cell numbers were assessed with a NucleoCounter® NC-100™ (Chemometec, Allerød, Denmark). In all experiments ~ 8×10^4 cells/cm^2 were seeded, washed with phosphate-buffered saline (PBS) (Invitrogen, Carlsbad, CA) after 24 hours and trypsinized (TripLE express, Invitrogen, Carlsbad, USA) for further processing. The percentage of adherent cells was calculated as follows: [Total cell count – detached cell count]/Total cell count. Light micrographic pictures were acquired using an IX71 inverted microscope (Olympus, Volketswil, Switzerland). Compound K00486 was applied at a concentration of 100nM to wildtype cells. For PIM1 overexpression human cDNA encoding PIM1 was subcloned into a pCMV-Tag2A expression vector (kind gift of Jürg Schwaller, Department of Biomedicine, University Hospital, Basel, Switzerland) and cell transfection was performed with 50ng of vector/reaction using a basic endothelial cells nucleofector kit in a Nucleofector II device (Amaxa Biosystems, Cologne, Germany) according to the manufacturers protocol.

Wound healing assay

Pim1 wildtype and knockout MAEC were grown to confluency in 6-well plates and wounded with a 200 µl pipette tip along a ruler. Wounded monolayers were washed three times with growth medium before further incubation. At the indicated time points (0, 4, 8 and 24 hours), monolayers were photographed 3 times for each well at 20x magnification. Wound width was measured on hard copy prints of the images. Individual cell paths were determined for leading-edge cells along five uniformly spaced lines along the wound edge. Initial wound at 0 hours was defined as 0% wound closed, total closure was defined as 100% wound closed.

Matrix exchange experiment

~ 8×10^4 cells/cm^2 wildtype and *Pim1*$^{-/-}$ MAECs were grown on 6-well plates (BD Biosciences, Franklin Lakes, NJ) for 24 hours. The cells were lysed with 25mM ammoniumhydroxyde (Sigma-Aldrich, St. Louis, MO) in PBS while leaving the extracellular matrix (ECM) intact and complete. To exclude remaining cells and cellular debris the plates were washed 3 times with PBS and total clearance was microscopically assessed. Wildtype cells grown on wildtype or *Pim1*$^{-/-}$ ECM for 24 hours were then trypsinized for 1, 2 or 3 minutes. To collect all the cells at each time point the cell layers were washed 3 times with PBS and the cell numbers in the collected supernatants were assessed and percentage of adherent cells was calculated as described above.

Immunoblotting

Total cell lysates were prepared using RIPA buffer as described before [19]. After SDS-PAGE, proteins were transferred onto polyvinylidene fluoride (PVDF) membrane (Millipore, Billerica, MA). The membrane was blocked with 4% skim milk powder in TBS-Tween solution or 4% BSA and probed with following antibodies: rabbit polyclonal anti-PIM1 (Cell Signaling Technology, Allschwil, Switzerland), primary mouse monoclonal to vinculin (abcam, Cambridge, MA), rabbit polyclonal anti-β-catenin (Cell Signalling Technology, Danvers, MA), rabbit polyclonal anti-T-cadherin (Sigma-Aldrich, St. Louis, MO), rabbit polyclonal anti-COL6A3 (Abnova Coorporation, Neihu, Taipei) and mouse monoclonal anti-β-actin (Sigma-Aldrich, St. Louis, MO). Anti-mouse or rabbit-HRP-conjugated IgGs (Cell Signalling Technology, Danvers, MA) were used for visualization of relevant proteins on X-ray films by a chemiluminescence reaction (Thermo Scientific, Waltham, MA).

Fluorescence imaging

The cells were fixed in 4% paraformaldehyde for 20 minutes at 37°C on coverslips (Karl Hecht AG, Sondheim, Germany) and then permeabilized with 0.5% Triton X-100 in PBS for 10 min. After blocking for 45 minutes with goat serum the cells were incubated with the following antibodies: primary mouse monoclonal to vinculin (abcam, Cambridge, MA), rabbit polyclonal anti-β-catenin (Cell Signalling Technology, Danvers, MA) and rabbit polyclonal COL6A3 antibody (Abnova Coorporation, Neihu, Taipei). After 3 washing steps cells were incubated with Alexa Fluor 555-conjugated secondary antibody (Invitrogen). F-actin was probed with Alexa Fluor 488 phalloidin and the nuclei were stained with Hoechst 33342 (Invitrogen). The coverslips were then mounted with FluorSave™ (Merck, Darmstadt, Germany) on glass slides (Thermo Scientific, Waltham, MA). Fluorescence imaging was performed using a Zeiss Axioskop 2 microscope (Zeiss, Oberkochen, Germany) and a confocal laser scanning microscope Leica SP5 (Leica, Wetzlar, Germany).

qRT-PCR

RNA was isolated using a RNAeasy Mini kit (Qiagen, Hilden, Germany), followed by a on column DNA digestion (Qiagen, Hilden, Germany). cDNA was transcribed from total RNA using Omniscript RT kit (Qiagen, Hilden, Germany) and random primers (Roche, Basel, Switzerland). To control for DNA contamination in the qRT-PCR, for each sample a control reaction missing reverse transcriptase was additionally amplified. Primers for microarray validation and genotyping wildtype and *Pim1*$^{-/-}$ cells were designed using Primer3 software (http://frodo.wi.mit.edu/primer3). Primers for validation were tested by cDNA dilution series to obtain optimal reaction conditions. qRT-PCR was performed using an iCycler iQ Real Time PCR Detection System (Biorad, Reinach, Switzerland) and iQ™ SYBR® Green Supermix (Biorad). Each representative reaction was loaded on an agarose gel for amplicon length analysis and additionally the melting curve was analyzed. The qRT-PCR was quantified as follows: $2^{-\Delta C_T} = C_T$ gene of interest – C_T *gapdh* [20].

Electric cell-substrate impedance sensing

Resistance measurements were performed using an ECIS Zθ apparatus (Applied Biopyhysics Inc.,Troy, NY) and either 8W1E arrays (Fig. 3) or 8W10E+ arrays (Fig. 4) both consisting of 8-wells with an area of 0.8 cm^2/well each and 1 or 40 gold electrodes with a diameter of 250 µm, respectively (Applied Biopyhysics Inc., Troy, NY). Before seeding cells, each well was preincubated with serum-free DMEM overnight followed by a 20 minutes coating with 0.1% gelatine gold (Carl Roth GmbH, Karlsruhe, Germany) and 0.9% sodium chloride in PBS, followed by 3 wash steps with serum free DMEM. 17 hours post transfection cells seeded

into 8W1E and 8W10E+ plates, respectively. The arrays in the measurement station were then placed in an incubator (37°C, 5% CO_2). Total resistance was measured in real-time at a frequency of 4 kHz. The complex impedance spectrum (Z, R, C) for each well was measured by applying an AC signal to the cells on the gold electrode, which output is measured over a frequency spectrum from 62.5 Hz to 64 kHz every 180 seconds by a second counter electrode. From this data the α^2 [Ω×cm^2] value and R_b [Ω×cm^2] was calculated using ECIS software (Applied Biopyhysics Inc.Troy, NY).

Microarray

Total RNA was processed with an Agilent whole mouse genome oligo microarray kit according to the manufacturers protocol (Agilent Technologies, Santa Clara, CA). Two coloured wildtype and *Pim1*$^{-/-}$ cRNA was hybridized to an Agilent Whole Mouse Genome 44K Microarray (Agilent Technologies, Santa Clara, CA) in triplicates. Analysis of hybridization images was done with CellsFeatureExtraction software (Agilent Technologies, Santa Clara, CA). The MetaCore™ analysis was performed with GeneGo software (Thomson Reuters, St. Joseph, MI). Complete microarray dataset is accessible at Gene Expression Omnibus database (GSE32059).

Statistical analysis

All statistical tests were performed using GraphPad Prism 5.04 for Windows (GraphPad software, San Diego, CA). For analysis of repeated measurements a two way Anova followed by a Bonferroni posttest was performed. Differences between two groups were evaluated using unpaired t-test and a p-value < 0.05 was considerd to be significant. To compare more than two groups one way anova followed by a Bonferroni posttest was done. a.u.c. was calculated over indicated time periods using GraphPad software. Data are represented as means ± s.e.m..

Results

Pim1 kinase deletion and inhibition slows endothelial cell detachment by trypsinization and increases cell adhesion

To investigate whether PIM1 has an influence on endothelial cell adhesion, confluent wildtype MAECs were treated with the imidazo[1,2-b]pyridazine compound K00486, a kinase inhibitor reported to inhibit human PIM1 kinase activity *in vitro* [21]. The resistance of the cell monolayer was recorded for 24 hours at a frequency of 4kHz using ECIS (Fig. 1A). Compared to control, we observed a significant increase of 80 ± 5 ohm of total resistance at 4kHz in cells treated with K00486, indicating the formation of a tighter cell monolayer. In parallel, MAECs were trypsinized 24 hours after seeding and the detachment process was followed in a time course (Fig. 1B): A significant delay in the detachment of inhibitor-treated versus untreated cells was observed as early as after 2 min (9±0.002% vs. 23±0.01% of detached cells in the supernatant) of trypsinization. The difference in detachment remained significant also for later time points (n=3, P<0.0001). Even though the PIM1 inhibitor K00486 has been suggested to inhibit only PIM1 kinase [21] we could not exclude unspecific inhibition by this compound.

To further substantiate our findings of increased endothelial cell adhesion after PIM1 inhibition, we isolated MAECs from mice deficient for PIM1 [22] and corresponding control mice. *Pim1* mRNA and protein expression in the isolated cells was assessed using quantitative real-time PCR (qRT-PCR) (Fig. 1C) and Western blotting (Fig. 1D) confirming the knockout of *Pim1*. Trypsin treatment of these cells for 0, 1, 2, 3, 4 and 5 minutes displayed an evident resistance to trypsinization and detachment of endothelial cells lacking PIM1. After 3 minutes, only 5±1% *Pim1*$^{-/-}$ cells were detached compared to 36±3% of wildtype cells (n=3, P<0.001). Similarly, after 5 minutes, *Pim1*$^{-/-}$ MAECs number in the supernatant was significantly lower (n=3, P<0.001) (Fig. 1E), which is also visible in corresponding micrographs (Fig. 1F).

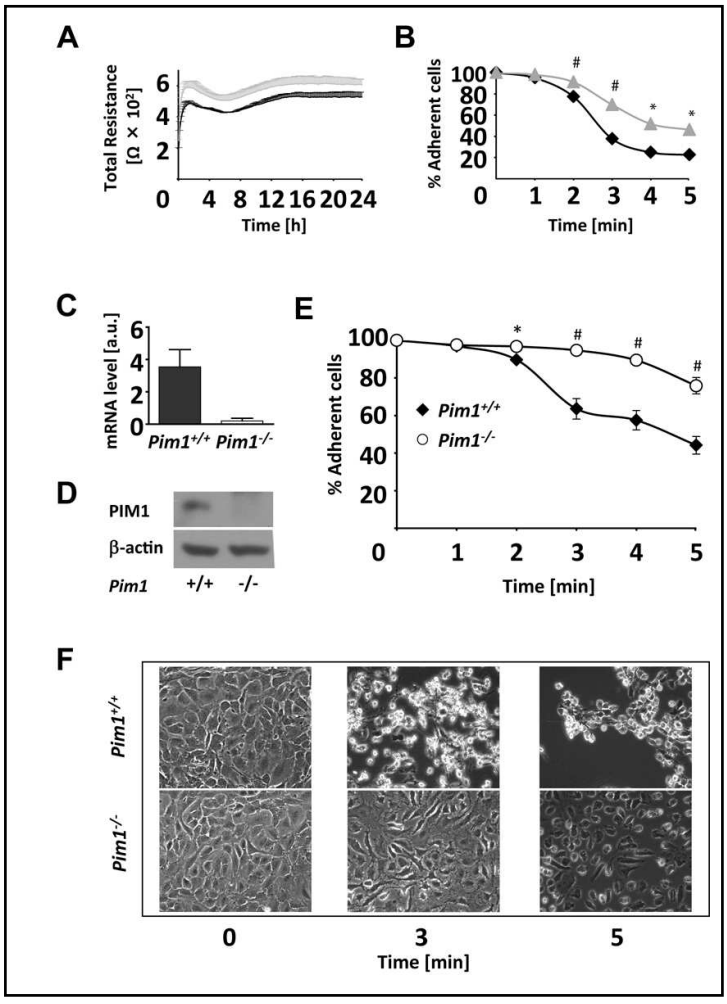

Fig. 1. Detachment of wildtype and *Pim1*$^{-/-}$ endothelial cells after trypsinization. (A) Time course of total resistance at 4 kHz of endothelial control and cells treated with K00486 over a period of 24 hours using ECIS. (B) Time course displaying number of cells detached represented as percentage of total adherent cells; control vs. cells treated with K00486. (C) Steady state mRNA expression levels of wildtype and *Pim1*$^{-/-}$ cells. (D) Corresponding Western blot of wildtype and *Pim1*$^{-/-}$ cells. (E) Time course displaying number of cells detached represented as percentage of total adherent cells; wildtype vs. *Pim1*$^{-/-}$cells. (F) Representative micrographs of wildtype and *Pim1*$^{-/-}$ cells before and after 3 and 5 minutes of trypsin treatment. β-actin was used as loading control. Black symbols indicate wildtype, grey wildtype with K00486 and open *Pim1*$^{-/-}$ cells. Data are represented as means ± s.e.m. (n=3). **P*<0.05, #*P*<0.0001.

Pim1$^{-/-}$ *decreases cell migration in a wound healing assay*

The differences in cell adhesion properties suggested that migratory response of *Pim1*$^{-/-}$ cells might be also affected. As a consequence we investigated cell motility (Fig. 2). Confluent wildtype and *Pim1*$^{-/-}$ endothelial monolayers were scratched and cell reinvasion into the wound was recorded over 24 hours. Quantification of the light micrographic pictures (Fig. 2A) revealed a 28.1±1.3% lower migration rate for *Pim1*$^{-/-}$ cells (n=5, *P*<0.00001) (Fig. 2B).

Pim1$^{-/-}$ *MAECs form tighter cell-substratum and cell-cell contacts*

Adhesion properties of wildtype and *Pim1*$^{-/-}$ cells were further analyzed using ECIS. Cells were seeded at confluence, and total resistance of cell layers was measured during 24 hours at a frequency of 4kHz. After 8 hours the cells reached confluency at the resistance value of 5600 ± 200 ohm for wildtype and 7800 ± 200 ohm for *Pim1*$^{-/-}$ cells (n=3, *P*<0.0001, Fig. 3A). The ECIS model allows differentiating between tightness of cell-cell contacts (R_b) and the strength of the cell-substratum adhesion (α^2) (Fig. 2B) [23, 24]. Area under the curve (a.u.c.) analysis for these parameters from 8 to 24 hours indicated a significant 2.3-fold of R_b (n=3, *P*<0.0001) and a 1.5-fold increase (n=3, *P*<0.0003) of α^2 respectively, in *Pim1*$^{-/-}$ cells (Fig. 3C). Thus, *Pim1* deletion in endothelial cells markedly and significantly strengthens cell-cell and cell-substratum adhesion as judged from the R_b and α^2 value.

Expression of PIM1 leads to a decrease in total resistance of endothelial Pim1$^{-/-}$ *cells*

To assess whether the hyper-adhesive properties of *Pim1*$^{-/-}$ cells might be indeed a consequence of loss of PIM1, we aimed to restore the phenotype by reintroduction of

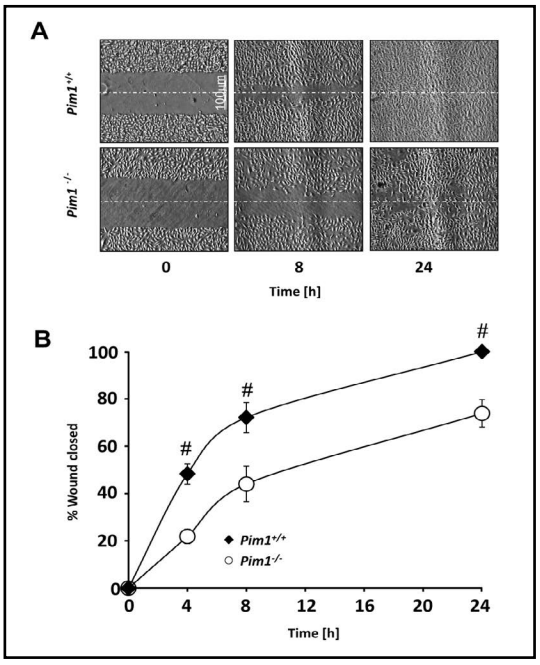

Fig. 2. Wound healing assay comparing wildtype and *Pim1*$^{-/-}$ MAEC. (A) Micrographs from wildtype (upper panel) and *Pim1*$^{-/-}$ (lower panel) cells 0, 8 and 24 hours after wounding. (B) Corresponding time course displaying the percentage of recolonized wound after 0, 4, 8 and 24 hours of cell migration. Black symbols indicate wildtype and open *Pim1*$^{-/-}$ cells. Data are represented as means ± s.e.m. (n=5). $^{\#}P<0.0001$.

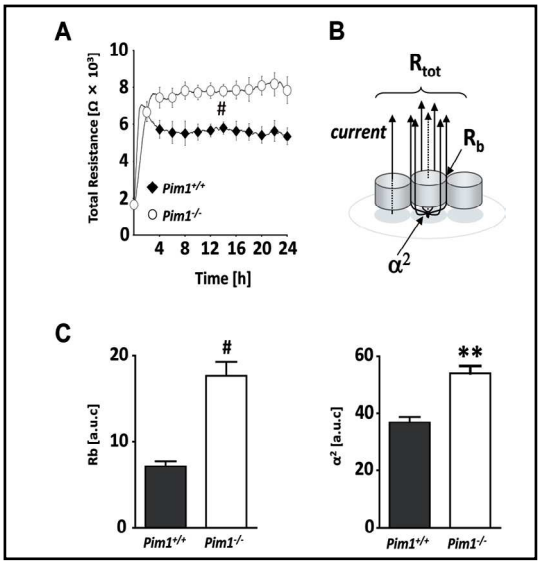

Fig. 3. Real-time monitoring of adhesion process and monolayer formation in wildtype and *Pim1*$^{-/-}$ MAECs. (A) Time course of total resistance at 4 kHz of endothelial wildtype and *Pim1*$^{-/-}$ endothelial cells over a period of 24 hours using ECIS. (B) Schematic view of an ECIS plate coated with cells. R_{tot}: total resistance (cell occupancy); R_b: resistance between the cells; α^2: cleft impedance parameter; (C) α^2 value and R_b value measurement of the confluent cell layers from 8 to 24 hours. Wildtype (filled symbols) and *Pim1*$^{-/-}$ (open symbols). Bars represent the area under the curve (a.u.c.) from 8 to 24 hours as means ± s.e.m. (n=3). $^{**}P<0.001$, $^{\#}P<0.0001$.

FLAG-*Pim1* cDNA into knockout cells. The amount of re-expressed FLAG-*Pim1* was determined by qRT-PCR and adjusted to similar levels of endogenous *Pim1* mRNA (Fig. 4A). We measured the total resistance of *Pim1*$^{-/-}$ cells expressing FLAG-*Pim1* cDNA, wildtype and *Pim1*$^{-/-}$ cells transfected with control plasmid during 24 hours. Attachment and plateau establishment were not significantly changed in *Pim1*$^{-/-}$ and *Pim1*$^{-/-}$ cells after FLAG-*Pim1* cDNA expression. However, after 16 hours of measurement the electrical resistance of cells expressing FLAG-*Pim1* significantly decreased compared to *Pim1*$^{-/-}$ cells. After 24 hours the rescue effect in *Pim1*$^{-/-}$ cells expressing FLAG-*Pim1* reached a maximum of approximately 40% reduction to wildtype resistance values (Fig. 4B).

Area under the curve analysis for the strength of cell-substratum adhesion and tightness of cell-cell contacts from 8 to 24 hours was calculated for wildtype, *Pim1*$^{-/-}$ and *Pim1*$^{-/-}$ cells expressing FLAG-*Pim1*. Reintroduction of FLAG-*Pim1* into wildtype or *Pim1*$^{-/-}$ cells did not affect α^2-value (Fig. 4C). However, the difference in the area under the curve (a.u.c.) for R_b between wildtype and *Pim1*$^{-/-}$ cells was reduced by 54% (n=3, $P<0.001$) when re-expressing FLAG-*Pim1* in *Pim1*$^{-/-}$ cells (Fig. 4D) Thus, reintroduction of *Pim1* cDNA into *Pim1*$^{-/-}$ MAEC restores R_b values to more than half of that of R_b wildtype levels.

Endothelial cell-cell junctions and focal adhesion structures are more pronounced in Pim1 knockout cells

β-catenin is a protein of the adherens junction complex and vinculin is an ubiquitary expressed protein involved in focal adhesion and also cell-cell contact formation [25, 26]. To validate the increased resistance in cell adherens junctions and focal adhesions

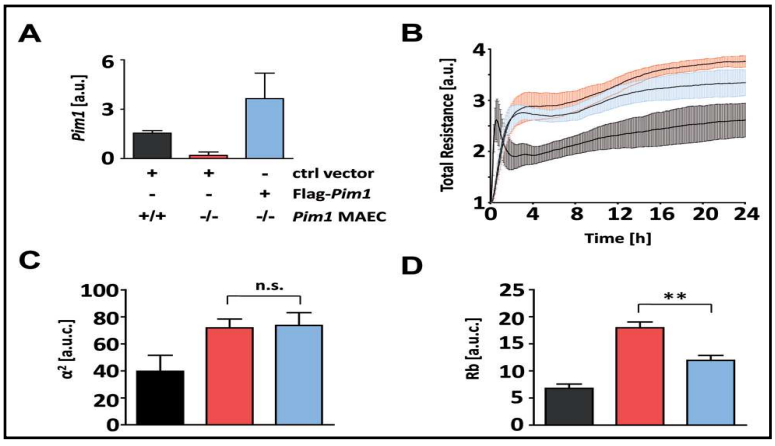

Fig. 4. ECIS analysis of *Pim1*$^{-/-}$ cells after FLAG-*Pim1* cDNA re-expression. (A) qRT-PCR of endogenous *Pim1* from wildtype and *Pim1*$^{-/-}$ cells and *Pim1*$^{-/-}$ cells transiently transfected with FLAG-*Pim1* cDNA, quantified with primers amplifying the FLAG sequence. (B) Determination of total resistance at 4 kHz during 24 hours from wildtype, *Pim1*$^{-/-}$ and FLAG-*Pim1* expressing *Pim1*$^{-/-}$ cells. (C) Area under the curve analysis of α^2 value from 8 to 24 hours of wildtype, *Pim1*$^{-/-}$ cells and *Pim1*$^{-/-}$ cells transfected with FLAG-*Pim1* cDNA. (D) Area under the curve analysis of R_b from 8 to 24 hours of wildtype, *Pim1*$^{-/-}$ cells and *Pim1*$^{-/-}$ cells transfected with FLAG-*Pim1* cDNA (left panel) with the corresponding resistance value curves (right panel). Resistance values were normalized to value 1 at time point 0 hours. Arbitrary units (a.u.) wildtype (black), *Pim1*$^{-/-}$ (red), *Pim1*$^{-/-}$ transfected with FLAG-*Pim1* (blue). Data are represented as means ± s.e.m. (n=3). $^{**}P<0.001$.

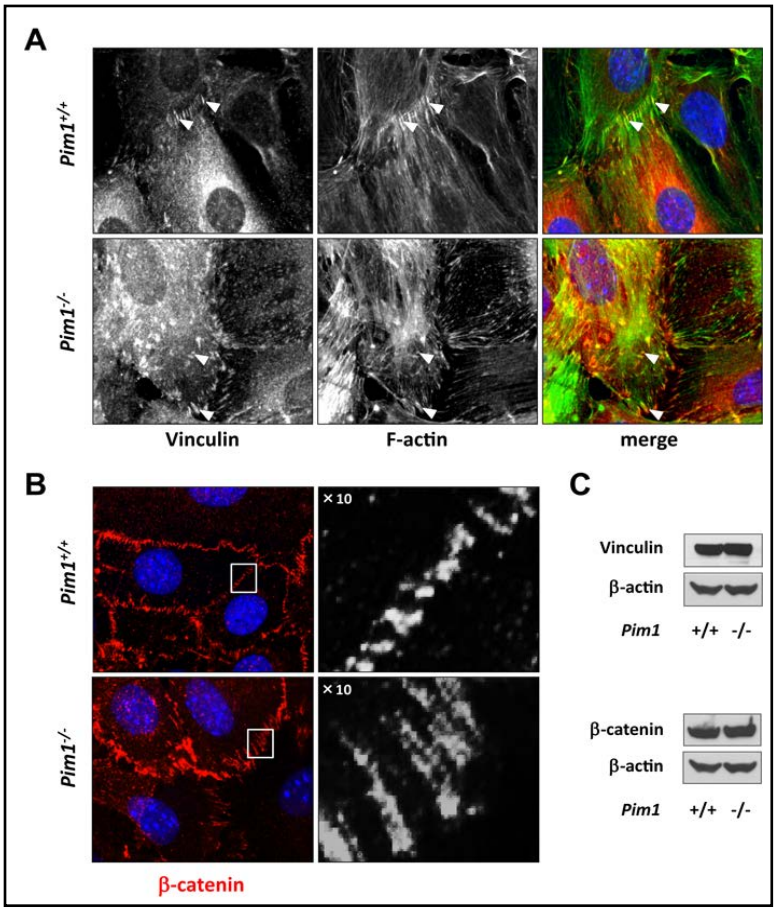

Fig. 5. Vinculin and β-catenin protein expression analysis. (A) Vinculin immunofluorescence images of MAEC, wildtype (upper left panel) vs. *Pim1*$^{-/-}$ (lower left panel) and F-actin staining of the corresponding area (middle panel). Merge of vinculin (red) and F-actin (green) images (left panel). (B) β-catenin (red) immunofluorescence images of wildtype (upper panel) and *Pim1*$^{-/-}$ (lower panel) MAEC. On the right a corresponding 10 times magnification of the area indicated by a white rectangle. (C) Western blot of vinculin (upper panel) and β-catenin (lower panel) from wildtype and *Pim1*$^{-/-}$ whole cell lysates. The nuclei are shown in blue. White arrows indicate the overlapping regions (yellow) (Total magnification ×100).

observed by ECIS, we assessed the protein expression levels of β-catenin and vinculin by immunofluorescence imaging and Western blot (Fig. 5). Fluorescence imaging disclosed a much more prominent vinculin patterning in *Pim1*$^{-/-}$ cells: The knockout cells formed more vinculin clusters around the cell (white arrows) (Fig. 5A left panel). Additionally also F-actin,

Table 1. Expression of differently expressed genes in *Pim1*$^{-/-}$ MAECs as identified by microarray analysis.

Gene Symbol	Acc. No.	Ratio	Gene Name	*P* -Value
Genes upregulated by *Pim-1* knockout				
Foxg1	NM_008241	214.9	*forkhead box G1*	0.0000227
Fhl1	NM_010211	199	*four and a half LIM domains 1*	0.000101
Col6a3	NM_009935	77.26	*collagen, type VI, alpha 3*	0.0006708
Sfrp2	NM_009144	35.64	*secreted frizzled-related protein 2*	0.001141
Ccdc68	NM_201362	31.66	*coiled-coil domain containing 68*	0.001582
Xlr4b	NM_021365	31.4	*X-linked lymphocyte-regulated 4B*	0.001146
Lhx9	NM_010714	30.16	*LIM homeobox protein 9*	0.0002769
Gsta1	NM_008181	21.62	*glutathione S-transferase*	0.001421
Col11a1	NM_007729	21.11	*collagen, type XI, alpha 1*	0.0001331
Serpine2	NM_009255	20.13	*serine (or cysteine) peptidase inhibitor, clade E, member 2*	2.89E-05
Genes downregulated by *Pim-1* knockout				
Eif2s3y	NM_012011	71.32	*eukaryotic translation initiation factor 2, subunit 3, structural gene Y-linked*	0.0008475
Gdf10	NM_145741	40.39	*growth differentiation factor 10*	0.004043
Thumpd1	NM_145585	29.63	*THUMP domain containing 1*	0.0007516
Svep1	NM_022814	25.24	*sushi, von Willebrand factor type A, EGF and pentraxin domain containing 1*	0.0004824
Ddx3y	NM_012008	24.28	*DEAD (Asp-Glu-Ala-Asp) box polypeptide 3, Y-linked*	0.002603
Serpina3g	NM_009251	22.76	*serine (or cysteine) peptidase inhibitor, clade A, member 3G*	0.004932
Tbx1	NM_011532	14.37	*T-box 1*	0.0001721
Svep1	NM_022814	13.87	*sushi, von Willebrand factor type A, EGF and pentraxin domain containing 1*	0.0003519
Cfh	NM_009888	12.60	*complement component factor h*	0.05249
Frzb	NM_011356	12.55	*frizzled-related protein*	0.003093

Table 2. Involvement of differently regulated genes in biological processes comparing *Pim1*$^{-/-}$ versus wildtype cells as analysed by GeneGo software (top down by *P*-value).

Biological Process		Description	*P* -Value
Cytoskeleton remodeling	:	TGF and WNT mediated cytoskeleton remodeling	2.03E-06
Signal transduction	:	Inhibition of Erk	3.03E-06
Cell adhesion	:	Histamine H1 receptor signaling in the interruption of cell barrier integrity	3.03E-06
Cell adhesion	:	Integrin-mediated cell adhesion and migration	5.34E-06
Immune response	:	CCR3 signaling in eosinophils	7.69E-06
Chemotaxis	:	Inhibitory action of lipoxins on IL-8- and Leukotriene B4-induced neutrophil migration	9.01E-06
Cytoskeleton remodeling	:	Role of PKA in cytoskeleton reorganisation	1.09E-05
Development	:	Role of HDAC and calcium/calmodulin-dependent kinase (CaMK) in control of skeletal myogenesis	1.47E-05
Muscle contraction	:	GPCRs in the regulation of smooth muscle tone	1.61E-05
Migration	:	Inhibitory action of Lipoxins on neutrophils	2.31E-05

which is bound by vinculin was stained (Fig. 5A middle panel). The overlay of vinculin and actin stainings visualizes the difference in the amount of focal adhesion clusters (Fig. 5A right panel). To investigate whether we also find distinct adherens junctions we additionally stained β-catenin in wildtype and knockout cells (Fig. 5B left panel). Indeed the β-catenin clusters were expanded in *Pim1*$^{-/-}$ cells, which is also visualized in a 10-times magnification in Fig. 5B right panel. Nevertheless we found no changes in overall protein expression of β-catenin and vinculin comparing wildtype and *Pim1*$^{-/-}$ cells (Fig. 5C).

Table 3. Genes involved in cell adhesion up- or downregulated in *Pim1*$^{-/-}$ cells. A cluster of genes which were found to be significantly regulated in the gene expression analysis was selected for further validation by qRT-PCR. (top down by ratio; P<0.05; †>0.05).

Gene Symbol	Acc. No.	Ratio	Gene Name	*P* -Value
Genes upregulated by *Pim-1* knockout				
Col6a3	NM_009935	77.3	*procollagen, type VI, alpha 3*	0.0067
Col11a1	NM_007729	21.1	*procollagen, type XI, alpha 1*	0.0001
Itgb4	NM_001005608	14.1	*integrin beta 4*	0.0037
Cdh13	NM_019707	11.4	*cadherine 13 / T-cadherine*	0.0001
Icam1 †	BC008626	5.9	*intercellular adhesion molecule 1*	0.0181
Itga7	NM_008398	3.8	*integrin alpha 7*	0.0001
Itga3	NM_013565	3	*integrin alpha 3*	0.0044
Jam2	NM_023844	2.609	*junction adhesion molecule 2*	0.0020
Genes downregulated by *Pim-1* knockout				
Svep1	NM_022814	25.64	*sushi, von Willebrand factor type A, EGF and pentraxin domain containing 1*	0.0005
Itga11	NM_176922	5.5	*integrin alpha 11*	0.0007
Adam23	NM_011780	4.9	*a disintegrin and metallopeptidase domain 23*	0.0020
Vcam1	NM_011693	3.1	*vascular cell adhesion molecule 1*	0.0009

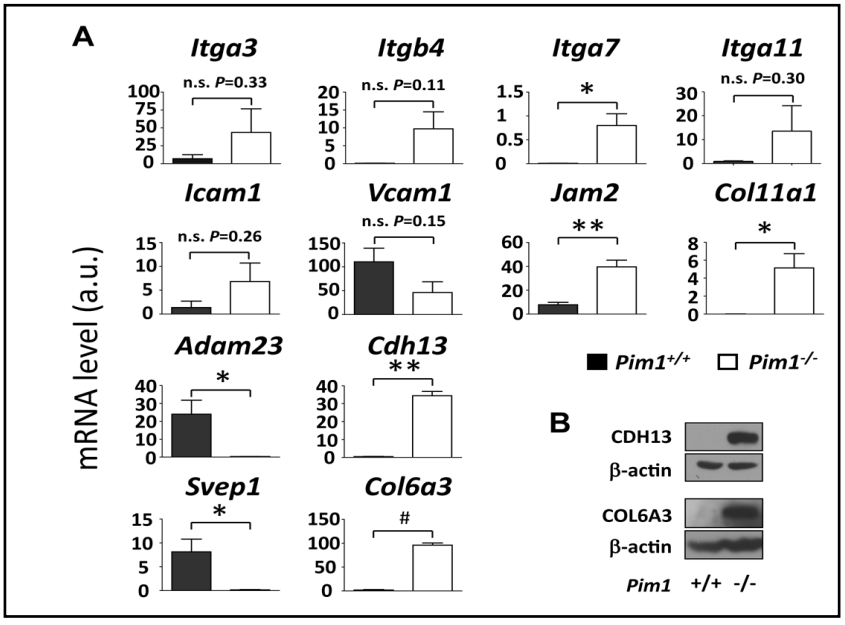

Fig. 6. Validation of the adhesion cluster using qRT-PCR. (A) mRNA from wildtype and *Pim1*$^{-/-}$ MAECs was isolated after 24 hours and steady state expression levels of indicated genes were validated by qRT-PCR. (B) Western blot of CDH13 and COL6A3 from wildtype and *Pim1*$^{-/-}$ whole cell lysates. Data are represented as means ± s.e.m. (n=3). *P<0.05, **P<0.001, #P<0.0001.

Gene expression analysis reveals importance of PIM1 in cell adhesion and cytoskeleton remodeling

To obtain a more global view of the ability of PIM1 to regulate cell adhesion we compared mRNA expression of wildtype and *Pim1*$^{-/-}$ cells using a two colour Agilent DNA microarray. Analysis of the gene expression data revealed 1598 significantly regulated genes (P<0.01) from which 61% were up- and 39% downregulated. The most regulated genes include *Foxg1* with a ratio of 200-fold upregulation and *Eif2s3* with a 70-fold downregulation (Table 1).

Single genes were summarized by their biological function using MetaCore™ analysis. Intriguingly, four out of ten most significantly regulated biological processes were computed as cell adhesion, migration and cytoskeleton remodeling (Table 2). This assignment is in line with our cell biological assessment.

A specific gene set involved in cell adhesion was selected for further validation (Table 3). Genes were selected 7 out of these 12 genes could be validated using qRT-PCR (Fig. 6A): the integrin family member *integrin alpha 7 (Itga7)*, the *junctional adhesion molecule 2 (Jam2)*, *T-cadherin* also known as *cadherin 13 (Cdh13)*, *a disintegrin and metalloproteinase*

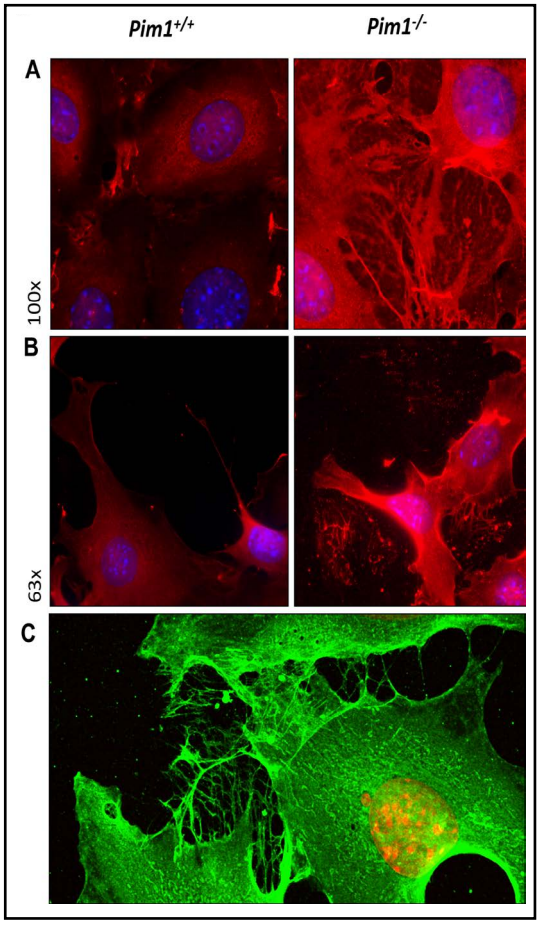

Fig. 7. *Pim1*$^{-/-}$ but not wildtype MAEC display deposits of COL6A3-positive fibre-like structures outside cells. (A) Representative micrographs of COL6A3 (red) and nuclear (blue) immunestaining in confluent wildtype (left) and *Pim1*$^{-/-}$ (right) MAEC (n=3, magnification 100x). (B) Representative micrographs of COL6A3 (red) and nuclear (blue) immunestaining in subconfluent wildtype (left) and *Pim1*$^{-/-}$ (right) MAEC (n=3, magnification 63x). (C) Laser scanning micrograph of COL6A3 (green) and nuclear (red) immunestaining in *Pim1*$^{-/-}$ (right) MAEC (magnification 100x).

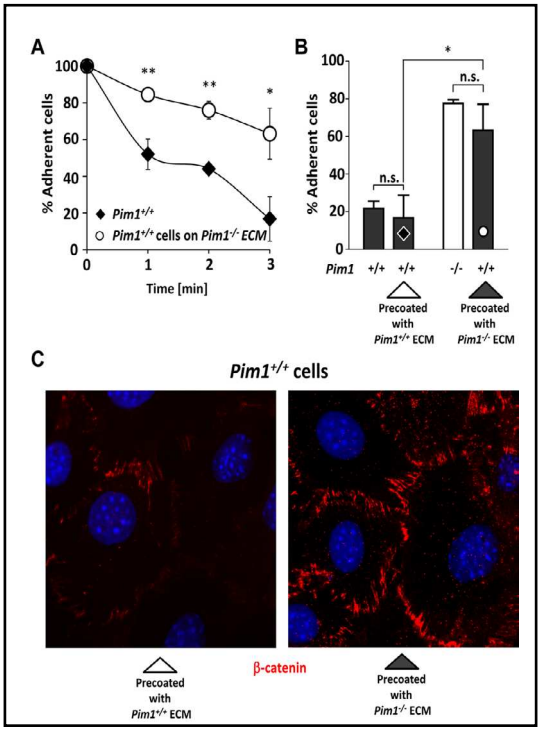

Fig. 8. Detachment of wildtype cells grown on wildtype or *Pim1*$^{-/-}$ ECM compared to wildtype and *Pim1*$^{-/-}$ cells after trypsinization. (A) Time course represented as a percentage of adherent wildtype cells after 0, 1, 2 and 3 minutes of trypsin treatment, grown either on wildtype or *Pim1*$^{-/-}$ ECM. Wildtype cells grown on wildtype ECM are shown as black symbols and wildtype cells grown on *Pim1*$^{-/-}$ ECM as open symbols. (B) Corresponding graph after 3 minutes of trypsinization compared to wildtype and *Pim1*$^{-/-}$ cells grown on their intrinsic ECM. Wildtype cells are shown as black, knockout cells as white bars, wildtype cells on wildtype ECM as black bars with a black diamond and wildtype cells on knockout ECM as black bars with an open circle. Data are represented as means ± s.e.m. (n=3). **P*<0.05, ***P*<0.001, $^{\#}$*P*<0.0001. (C) Immunofluorescent staining of β-catenin (red) and nuclei (DAPI, blue) of wildtype MAEC cultured on matrices deposited by wildtype MAEC (micrograph on the left) and by *Pim1*$^{-/-}$ MAEC (micrograph on the right; magnification 63x, n=3).

domain-containing protein 23 (Adam23), the extracellular matrix proteins *collagen type VI, alpha 3 (Col6a3)*, *collagen type XI, alpha 1 (Col11a1)* and *sushi, von Willebrand factor type A, epidermal growth factor and pentraxin domain containing 1 (Svep1)* which belongs to a new group of membrane proteins involved in cell adhesion [27]. The most significantly regulated genes also displaying the highest mRNA expression levels in *Pim1*$^{-/-}$ cells were identified as *Col6a3* (fold induction = 51.6; *P*<0.0001), and *Cdh13* (fold induction = 81.9; *P*<0.0002) (Fig. 6), both upregulated in *Pim1*$^{-/-}$ cells. Figure 6B shows protein expression levels of CDH13 and COL6A3, both proteins either involved in cell-cell or cell substratum adhesion.

Pim1$^{-/-}$-deposited matrix induces adhesion characteristics of Pim1$^{-/-}$ cells in wildtype cells

Extracellular matrix deposition and composition is of fundamental importance in cell adhesion and migration [28]. We found significantly different gene expression of matrix components and cell-matrix receptors, such as collagens and integrins. COL6A3 as the most strongly and significantly expressed matrix component was further examined by immunestaining. We found that confluent *Pim1$^{-/-}$* but not wildtype MAEC expressed COL6A3 positive bundles inside the cells, extending in network-like structures on top of endothelial cells (Fig. 7A, right micrograph). Furthermore, *Pim1$^{-/-}$* but not wildtype MAEC deposited fibre-like structures containing COL6A3 between cells accumulating on the cell-free culture plate surface (Fig. 7B, right micrograph and Fig. 7C).

We therefore aimed at determining whether the adhesion properties of *Pim1$^{-/-}$* cells also depend on this specific ECM deposition. Wildtype cells were cultivated on ECM deposited by wildtype or *Pim1$^{-/-}$* cells (Fig. 8A). Trypsin treatment of these confluent cells for 0, 1, 2 and 3 minutes displayed a marked delay of the detachment of wildtype endothelial cells cultured on matrix deposited by *Pim1$^{-/-}$* cells (Fig. 8A). Wildtype cells remained attached to the *Pim1$^{-/-}$* matrix to 84±1% in contrast to 52±8% on the wildtype matrix after 1 minute of trypsin treatment and three PBS washing steps (n=3, $P<0.003$). After three minutes and three PBS washing steps 63.2±13% of wildtype cells were remained attached to the *Pim1$^{-/-}$* matrix whereas only 16.8±12% of wildtype cells remained attached to the wildtype matrix (n=3, $P<0.02$).

To compare the degree to which *Pim1$^{-/-}$* deposited matrix was able to induce adhesion characteristics of *Pim1$^{-/-}$* cells in wildtype cells, we performed trypsinization experiments with confluent wildtype and *Pim1$^{-/-}$* cells which were washed three times after three minutes of trypsin treatment. Again, supernatant was collected and cells counted. The washing steps decreased the number of wildtype MAEC remaining attached to the culture dish (21.7±1.8%), whereas *Pim1$^{-/-}$* cells still resisted trypsinization (77.5±0.9%, n=5, $P<0.0003$) (Fig. 8B). The percentage of *Pim1$^{-/-}$* cells remaining attached to the substratum was similar and statistically not different compared to the percentage of wildtype cells remaining attached to the *Pim1$^{-/-}$* deposited matrix after three minutes of trypsin treatment ($P=0.47>0.05$, n=3) (Fig. 8B). Finally, we investigated, whether *Pim1$^{-/-}$* cell-deposited matrix was sufficient to induce structural changes in adherens junctions of wildtype MAEC as observed in *Pim1$^{-/-}$* cells (see Fig. 5B). Indeed, when cultivating wildtype MAEC on *Pim1$^{-/-}$* cell-deposited matrix and staining confluent cultures, we observed enhanced β-catenin containing structures at cell-cell borders (Fig. 8C).

Thus, ECM deposited by *Pim1$^{-/-}$* cells is sufficient to mediate a hyperadhesive phenotype similar to that of *Pim1$^{-/-}$* cells with respect to cell detachment and adherens junction strengthening.

Discussion

Here we report that PIM1 plays a distinct role in endothelial cell-cell cohesion and cell-matrix adhesion. We demonstrate that *Pim1* deletion and kinase inhibition slows endothelial cell detachment by trypsinization and increases total electrical resistance across the endothelial monolayer. Reintroduction of *Pim1* cDNA into *Pim1$^{-/-}$* cells partially but significantly restored electrical resistance to wildtype levels. Furthermore, *Pim1* deletion in endothelial cells markedly reduced cell motility as shown in wound healing assays. This finding is consistent with an earlier report using cells derived from human prostate cancer or squamo-cellular carcinoma where *Pim1* silencing decreased wound healing *in vitro* [9]. We therefore conclude that modulation of endothelial cell adhesion by *Pim1* deletion, kinase inhibition and *Pim1* cDNA reintroduction into *Pim1$^{-/-}$* cells is actually *Pim1*-specific and most likely requires its classical serine-threonine kinase activity, as suggested earlier by Santio et al., since a similar PIM1 kinase inhibitor in human cancer cells slowed down cell motility [9].

Cell migration is a complex, tightly regulated process that involves the dynamic formation and disassembly of distinct adhesion complexes [29, 30]. We therefore further dissected the characteristics of endothelial cell adhesion modulation by differentiating electrical resistance values and found that both cell-cell cohesion and cell-substrate adhesion were reinforced by *Pim1* deletion.

The intracellular domain of the adherens junctions effector protein VE–cadherin contains a distal binding site for β-catenin. β-catenin is linked to α-catenin, which may further interact with the cytoskeleton via α-actinin and vinculin [26, 31]. Finally, integrins directly adhere to the matrix substratum and connect to talin and vinculin, [32]. Interestingly, *Pim1*$^{-/-}$ cells exhibited more vinculin positive focal adhesion structures that spread the entire endothelial cell surface, whereas wildtype cells displayed less vinculin positive streaks that were predominantly located laterally at cell junctions. Furthermore, *Pim1*$^{-/-}$ cells displayed abnormally enlarged β-catenin positive structures at cell-cell junctions than usually found in wildtype endothelial cells. Thus, *Pim1* deletion reinforced connection complexes between cell to cell junctions and focal adhesion structures, which might mechanically increase intercellular forces and tension [33]. While *Pim1* deletion did not change overall β-catenin and vinculin protein levels, gene expression analysis demonstrated significant and strong regulation of matrix components (*Col6a, Col11a*) and cell to matrix (*Itga7*) and cell to cell attachment (*Cdh13, Jam2*) modulating genes. MetaCore™ analysis of all genes modulated by *Pim1* deletion revealed WNT-mediated cytoskeleton remodeling as the most significantly regulated biological process.

Pim1$^{-/-}$ but not wildtype cells deposited a specific, COL6A3-containing matrix in fibre-like structures on culture dish surfaces: Intriguingly, ECM deposited by *Pim1*$^{-/-}$ cells alone was sufficient to induce *Pim1*$^{-/-}$ adhesion characteristics in wildtype cells which may be interpreted as one of the early events in the establishment of the *Pim1*$^{-/-}$ adhesion phenotype. Matrix-integrin mediated signals are transduced by the focal adhesion kinase (FAK) [31]. Thus, enhanced matrix-integrin interactions in *Pim1*$^{-/-}$ cells may increase vinculin-containing focal adhesion structures and modulate FAK signaling. Observations in different model systems suggest a complex and dynamic cross-talk between the focal adhesion kinase and the WNT-signaling pathway [34, 35]. Canonical WNT-signalling promotes dissociation of β-catenin from junctional complexes to the nucleus, which also results in reduced cell-cell adhesion in tumorigenesis [36]. As we show in Fig. 5B, *Pim1*$^{-/-}$ MAEC display pronounced β-catenin clusters at the cell to cell borders, which could be explained by reduced WNT-signalling in these cells. This is also demonstrated in FAK kinase dead mutant mice where vascular permeability and angiogenic growth factor VEGF failed to induce dissociation of β-catenin from adherens junction complexes [37]. Intriguingly we found that *Pim1*$^{-/-}$ cell-deposited matrix also enhanced β-catenin-containing structures at cell-cell contacts. Therefore, we assume that matrix-induced signaling may repress WNT signaling in *Pim1*$^{-/-}$ endothelium preventing redistribution of β-catenin from adherens junctions to the nucleus, thereby enhancing cell-cell cohesion.

Taken together, we demonstrate a distinct novel role of PIM1 in the regulation of endothelial cell-cell cohesion and cell-matrix adhesion, which likely involves a matrix-initiated response involving collagen, alteration in vinculin-containing focal adhesion structures and pronounced β-catenin-containing junctional complexes. This is accompanied by alterations in cell adhesion gene regulation. A hyperadhesive endothelial *Pim1*$^{-/-}$ phenotype might be useful to promote endothelial barrier integrity, restrict angiogenesis in growing tumors and impede invasion and metastatic spread of malignant cells through the endothelial monolayer.

Competing interests

No competing interests

Acknowledgements

This work was supported by a grant from the Swiss National Science Foundation to Edouard J. Battegay and from matching funds and the Jubiläumsstiftung of the University of Zürich. We thank A. Berns and M.C. Nawijn who kindly provided the FVB/N wildtype and *Pim1*$^{-/-}$ mouse strains (The Netherlands Cancer Institute, Amsterdam, Netherlands). We thank Thérèse J. Resink who kindly provided us the T-Cad antibody. We also would like to thank Ana I. Perez Dominguez, Marlen Damjanović, Katja Drägert for helping with the RT-qPCR (University Hospital Zürich). Last but not least we thank Hubert Rehrauer (Functional genomics center Zürich, Switzerland) for his support with the microarray.

References

1 Qian KC, Wang L, Hickey ER, Studts J, Barringer K, Peng C, Kronkaitis A, Li J, White A, Mische S, Farmer B: Structural basis of constitutive activity and a unique nucleotide binding mode of human Pim-1 kinase. J Biol Chem 2005;280:6130-6137.

2 Breuer ML, Cuypers HT, Berns A: Evidence for the involvement of pim-2, a new common proviral insertion site, in progression of lymphomas. EMBO J 1989;8:743-748.

3 Feldman JD, Vician L, Crispino M, Tocco G, Marcheselli VL, Bazan NG, Baudry M, Herschman HR: KID-1, a protein kinase induced by depolarization in brain. J Biol Chem 1998;273:16535-16543.

4 van der Lugt NM, Domen J, Verhoeven E, Linders K, van der Gulden H, Allen J, Berns A: Proviral tagging in E mu-myc transgenic mice lacking the Pim-1 proto-oncogene leads to compensatory activation of Pim-2. EMBO J 1995;14:2536-2544.

5 Mikkers H, Nawijn M, Allen J, Brouwers C, Verhoeven E, Jonkers J, Berns A: Mice deficient for all PIM kinases display reduced body size and impaired responses to hematopoietic growth factors. Mol Cell Biol 2004;24:6104-6115.

6 Brault L, Gasser C, Bracher F, Huber K, Knapp S, Schwaller J: PIM serine/threonine kinases in the pathogenesis and therapy of hematologic malignancies and solid cancers. Haematologica 2010;95:1004-1015.

7 Tanaka S, Kitamura T, Higashino F, Hida K, Ohiro Y, Ono M, Kobayashi M, Totsuka Y, Shindoh M: Pim-1 activation of cell motility induces the malignant phenotype of tongue carcinoma. Mol Med Report 2009;2:313-318.

8 Warnecke-Eberz U, Bollschweiler E, Drebber U, Metzger R, Baldus SE, Holscher AH, Monig S: Prognostic impact of protein overexpression of the proto-oncogene PIM-1 in gastric cancer. Anticancer Res 2009;29:4451-4455.

9 Santio NM, Vahakoski RL, Rainio EM, Sandholm JA, Virtanen SS, Prudhomme M, Anizon F, Moreau P, Koskinen PJ: Pim-selective inhibitor DHPCC-9 reveals Pim kinases as potent stimulators of cancer cell migration and invasion. Mol Cancer 2010;9:279.

10 Nawijn MC, Alendar A, Berns A: For better or for worse: the role of Pim oncogenes in tumorigenesis. Nat Rev Cancer 2011;11:23-34.

11 Zippo A, De Robertis A, Bardelli M, Galvagni F, Oliviero S: Identification of Flk-1 target genes in vasculogenesis: Pim-1 is required for endothelial and mural cell differentiation in vitro. Blood 2004;103:4536-4544.

12 Miles FL, Pruitt FL, van Golen KL, Cooper CR: Stepping out of the flow: capillary extravasation in cancer metastasis. Clin Exp Metastasis 2008;25:305-324.

13 Folkman J: Angiogenesis in cancer, vascular, rheumatoid and other disease. Nat Med 1995;1:27-31.

14 Sokmen S, Sarioglu S, Fuzun M, Terzi C, Kupelioglu A, Aslan B: Prognostic significance of angiogenesis in rectal cancer: a morphometric investigation. Anticancer Res 2001;21:4341-4348.

15 Al-Mehdi AB, Tozawa K, Fisher AB, Shientag L, Lee A, Muschel RJ: Intravascular origin of metastasis from the proliferation of endothelium-attached tumor cells: a new model for metastasis. Nat Med 2000;6:100-102.

16 Teicher BA, Fricker SP: CXCL12 (SDF-1)/CXCR4 pathway in cancer. Clin Cancer Res 2010;16:2927-2931.
17 Weis S, Cui J, Barnes L, Cheresh D: Endothelial barrier disruption by VEGF-mediated Src activity potentiates tumor cell extravasation and metastasis. J Cell Biol 2004;167:223-229.
18 Humar R, Kiefer FN, Berns H, Resink TJ, Battegay EJ: Hypoxia enhances vascular cell proliferation and angiogenesis in vitro via rapamycin (mTOR)-dependent signaling. FASEB J 2002;16:771-780.
19 Li W, Petrimpol M, Molle KD, Hall MN, Battegay EJ, Humar R: Hypoxia-induced endothelial proliferation requires both mTORC1 and mTORC2. Circ Res 2007;100:79-87.
20 Schmittgen TD, Lee EJ, Jiang J, Sarkar A, Yang L, Elton TS, Chen C: Real-time PCR quantification of precursor and mature microRNA. Methods 2008;44:31-38.
21 Pogacic V, Bullock AN, Fedorov O, Filippakopoulos P, Gasser C, Biondi A, Meyer-Monard S, Knapp S, Schwaller J: Structural analysis identifies imidazo[1,2-b]pyridazines as PIM kinase inhibitors with in vitro antileukemic activity. Cancer Res 2007;67:6916-6924.
22 Laird PW, van der Lugt NM, Clarke A, Domen J, Linders K, McWhir J, Berns A, Hooper M: In vivo analysis of Pim-1 deficiency. Nucleic Acids Res 1993;21:4750-4755.
23 Giaever I, Keese CR: Micromotion of mammalian cells measured electrically. Proc Natl Acad Sci U S A 1991;88:7896-7900.
24 Bagnaninchi PO, Drummond N: Real-time label-free monitoring of adipose-derived stem cell differentiation with electric cell-substrate impedance sensing. Proc Natl Acad Sci U S A 2011;108:6462-6467.
25 Nyqvist D, Giampietro C, Dejana E: Deciphering the functional role of endothelial junctions by using in vivo models. EMBO Rep 2008;9:742-747.
26 Wallez Y, Huber P: Endothelial adherens and tight junctions in vascular homeostasis, inflammation and angiogenesis. Biochim Biophys Acta 2008;1778:794-809.
27 Shefer G, Benayahu D: SVEP1 is a novel marker of activated pre-determined skeletal muscle satellite cells. Stem Cell Rev 2010;6:42-49.
28 Costa P, Parsons M: New insights into the dynamics of cell adhesions. Int Rev Cell Mol Biol 2010;283:57-91.
29 Webb DJ, Brown CM, Horwitz AF: Illuminating adhesion complexes in migrating cells: moving toward a bright future. Curr Opin Cell Biol 2003;15:614-620.
30 Wimmer R, Cseh B, Maier B, Scherrer K, Baccarini M: Angiogenic sprouting requires the fine tuning of endothelial cell cohesion by the Raf-1/Rok-alpha complex. Dev Cell 2012;22:158-171.
31 Quadri SK: Cross talk between focal adhesion kinase and cadherins: role in regulating endothelial barrier function. Microvasc Res 2012;83:3-11.
32 Bakolitsa C, Cohen DM, Bankston LA, Bobkov AA, Cadwell GW, Jennings L, Critchley DR, Craig SW, Liddington RC: Structural basis for vinculin activation at sites of cell adhesion. Nature 2004;430:583-586.
33 Chervin-Petinot A, Courcon M, Almagro S, Nicolas A, Grichine A, Grunwald D, Prandini MH, Huber P, Gulino-Debrac D: Epithelial protein lost in neoplasm (EPLIN) interacts with alpha-catenin and actin filaments in endothelial cells and stabilizes vascular capillary network in vitro. J Biol Chem 2012;287:7556-7572.
34 Fonar Y, Frank D: FAK and WNT signaling: the meeting of two pathways in cancer and development. Anticancer Agents Med Chem 2011;11:600-606.
35 Pandur P, Maurus D, Kuhl M: Increasingly complex: new players enter the Wnt signaling network. Bioessays 2002;24:881-884.
36 Fu Y, Zheng S, An N, Athanasopoulos T, Popplewell L, Liang A, Li K, Hu C, Zhu Y: β-catenin as a potential key target for tumor suppression. Int J Cancer 2011;129:1541-1551.
37 Chen XL, Nam JO, Jean C, Lawson C, Walsh CT, Goka E, Lim ST, Tomar A, Tancioni I, Uryu S, Guan JL, Acevedo LM, Weis SM, Cheresh DA, Schlaepfer DD: VEGF-induced vascular permeability is mediated by FAK. Dev Cell 2012;22:146-157.